Geochemistry, Geophysics, Geosystems

RESEARCH ARTICLE
10.1029/2020GC009028

Key Points:
- Plastic overprint of brittle precursory structures is efficient in the presence of water-rich fluids triggering reactions
- Fluid influx and subsequent reaction in the wall rock result in the widening of the zone accommodating strain

Correspondence to:
S. Incel,
sarah.incel@rub.de

Citation:
Incel, S., Renner, J., & Jamtveit, B. (2020). Evolution of brittle structures in plagioclase-rich rocks at high-pressure and high-temperature conditions—Linking laboratory results to field observations. *Geochemistry, Geophysics, Geosystems*, *21*, e2020GC009028. https://doi.org/10.1029/2020GC009028

Received 12 MAR 2020
Accepted 25 JUN 2020
Accepted article online 29 JUN 2020

Evolution of Brittle Structures in Plagioclase-Rich Rocks at High-Pressure and High-Temperature Conditions—Linking Laboratory Results to Field Observations

Sarah Incel[1,2], Jörg Renner[2], and Bjørn Jamtveit[1]

[1]Physics of Geological Processes, The Njord Centre, Department of Geosciences, University of Oslo, Oslo, Norway, [2]Institute for Geology, Mineralogy, and Geophysics, Ruhr University Bochum, Bochum, Germany

Abstract Plagioclase-rich granulites exposed on the Lofoten archipelago, Northern Norway, display strain localization in pseudotachylytes as well as ductile shear zones that formed under similar high-pressure and high-temperature conditions. Pseudotachylytes or pseudotachylyte networks reveal no or very little hydration, whereas ductile shear zones reveal significant hydration. We combine these observations from the field with experimental results to characterize the structural evolution of brittle faults in plagioclase-rich rocks at conditions of the lower continental crust. We performed a series of deformation experiments on intact granulite samples prepared from a natural granulite sample at 2.5 GPa confining pressure, a strain rate of 5×10^{-5} s^{-1}, and temperatures of 700°C and 900°C to total strains of ~7–8% and ~33–36%. Samples were either deformed "as-is" or with ~1 wt.% H_2O added. Striking similarities between the experimental and natural microstructures suggest that the transformation of precursory brittle structures into ductile shear zones at eclogite-facies conditions is most effective in samples deformed with added water triggering reaction and subsequent plastic deformation of the products along the faults and in the adjacent wall-rock.

Plain Language Summary Pseudotachylytes and ductile shear zones, both reflecting the localization of strain, can be found in high-pressure, high-temperature rocks of the lower continental crust, for example, in the Lofoten archipelago, Northern Norway. In contrast to the pseudotachylyte mineral assemblage, ductile shear zones show a significant amount of hydrous minerals. To experimentally investigate the influence of water-rich fluids on the evolution of brittle structures at conditions of the lower continental crust, we conducted deformation experiments on intact granulite samples and compared our laboratory results to natural microstructures of the Lofoten samples. To investigate the microstructural evolution of the experimental samples, we terminated the tests at ~7–8% and 33–36% axial shortening. We studied the importance of water for the microstructural evolution of the samples by either deforming natural samples "as-is" or by adding approximately 1 wt.% H_2O. In addition, we tested the influence of temperature by performing the experiments at 700°C and 900°C. All tests were conducted at a confining pressure of 2.5 GPa and a strain rate of 5×10^{-5} s^{-1}. The experimental microstructures demonstrate that the transformation of brittle structures to ductile shear zones is most effective in samples deformed with added water.

1. Introduction

The rheology of rocks and especially the localization of strain in the lower continental crust is of great importance since the flow behavior of the lower continental crust strongly influences the deformation behavior of the entire continental lithosphere. From previous studies, it has become increasingly clear that plagioclase-rich rocks deformed at pressure (P) and temperature (T) conditions prevailing at depths of the lower continental crust, that is, ~650°C to 800°C and 1.6 to 2.2 GPa (Austrheim & Griffin, 1985; Bhowany et al., 2017), show a mixture of brittle and plastic deformation denoted as semibrittle behavior (McLaren & Pryer, 2001; Okudaira et al., 2015; Stünitz et al., 2003; Tullis & Yund, 1987, 1992). Microstructural analysis of garnet grains in mylonitic micaschists from the Sesia Zone, Western Alps, revealed that lower crustal rocks show evidence for cataclasis due to high transient stresses and strain rates probably occurring during earthquakes, as well as plastic creep probably characterizing postseismic or interseismic deformation (Trepmann & Stöckhert, 2002). The occurrence of pseudotachylytes constitutes evidence for brittle

deformation in rocks of the lower continental crust, for example, in the Norwegian Caledonides (Bhowany et al., 2017; Jin et al., 2002; Kim et al., 2013; Marshall & McLaren, 1977; Milsch & Scholz, 2005; Tribaudino et al., 2010) and in the Musgrave Block, Central Australia (Hawemann, Mancktelow, Pennacchioni, et al., 2019, Hawemann, Mancktelow, Wex, et al., 2019, 2018). Pseudotachylytes and associated deformation features in the adjacent wall rock highlight extreme transient stresses and strain rates that are believed to occur during dynamic rupture propagation (Austrheim et al., 2017; Hawemann, Mancktelow, Wex, et al., 2019, Hawemann, Mancktelow, Pennacchioni, et al., 2019, 2018; Jamtveit et al., 2019; Petley-Ragan et al., 2019, 2018). Throughout the Norwegian Caledonides, pseudotachylytes often occur in close spatial relation with ductile shear zones that both form under similar *P-T* conditions (Austrheim, 1986; Austrheim & Griffin, 1985; Campbell & Menegon, 2019; Jamtveit et al., 1990, 2019; John et al., 2009; Jolivet et al., 2005; Lund et al., 2004; Lund & Austrheim, 2003; Menegon et al., 2013, 2017; Raimbourg et al., 2005). Because of the close spatial occurrence of brittle faults and ductile shear zones at a variety of locations worldwide, it has been suggested that ductile shear zones can nucleate on preexisting brittle faults (Guermani & Pennacchioni, 1998; Mancktelow & Pennacchioni, 2005; Menegon et al., 2017; Pennacchioni & Mancktelow, 2007; Pittarello et al., 2012; Segall & Simpson, 1986; Tullis et al., 1990).

In experiments covering a broad range of experimental conditions of 2.5 GP, 700°C to 1100°C, and strain rates of 10^{-4} to 10^{-6} s^{-1} mimicking conditions of the lower continental crustal, prefaulted and intact plagioclase-rich samples deform mainly by dislocation creep, causing the transformation of brittle faults to narrow ductile shear zones (Tullis et al., 1990; Tullis & Yund, 1985). In nature, this transformation of brittle structures to ductile shear zones at elevated pressures and temperatures may cause plastic overprinting of pseudotachylytes during further deformation and exhumation (Kirkpatrick & Rowe, 2013; Price et al., 2012; Sibson & Toy, 2006). However, pseudotachylytes formed at conditions of the lower continental crust are also reported from several localities. Field observations from the Lofoten archipelago, Northern Norway (Figure 1) show that rock volumes containing ductile shear zones invariably show a significant extent of hydration, whereas rock volumes with pseudotachylytes or pseudotachylyte networks exhibit none or limited hydration. Preferential preservation of pseudotachylytes in dry environments suggests a direct link between the availability of fluids and the extent of plastic overprint of brittle precursors.

In the present study, we conducted experiments to investigate the impact of water on the transformation of brittle structures to ductile shear zones at eclogite-facies conditions. Furthermore, to better understand the evolution of brittle structures, that is, pseudotachylytes, in nature, we compare the experimentally produced microstructures to natural microstructures from rocks of the lower continental crust from the Lofoten archipelago, Northern Norway.

2. Plagioclase Breakdown at Eclogite-Facies Conditions

At eclogite-facies conditions, plagioclase decomposes to zoisite ± garnet, jadeite, quartz, and kyanite (Goldsmith, 1980, 1981). In the presence of water-rich fluids, zoisite will form, while garnet growth requires low water activities. Experiments demonstrated that in the presence of minor amounts of a water-rich fluid, the kinetics of nucleation and growth of zoisite is fast compared to that of quartz, garnet, and kyanite (Wayte et al., 1989). Although eclogitization of plagioclase-rich granulite involves hydration of the reactant, the solid volume change is negative ($\Delta V_{solid} \approx -14\%$). Natural plagioclase often contains minor amounts of potassium (K) in an orthoclase (Or) component. When plagioclase contains K, muscovite or sanidine will nucleate and grow during eclogitization, depending on the amount of water present, with muscovite forming at higher water contents.

3. Localities and Sample Collection

Three samples representing localized deformation in rocks of the lower continental crust were collected from two different localities on the Lofoten Islands, Northern Norway, near Hamnøya on Moskenesøya (67°56′58.1″N 13°08′14.9″E) and near Ramberg on Flakstadøya (68°06′16.3″N 13°15′33.3″E; Figure 1). A hand specimen was collected from mangeritic rock at the Hamnøya roadcut (Figure 2a). The geological map from Griffin et al., 1978 indicates that the area around Hamnøya should be dominated by paragneisses (Figure 1). However, due to the presence of Ti-magnetite, we conclude that they represent granulite-facies

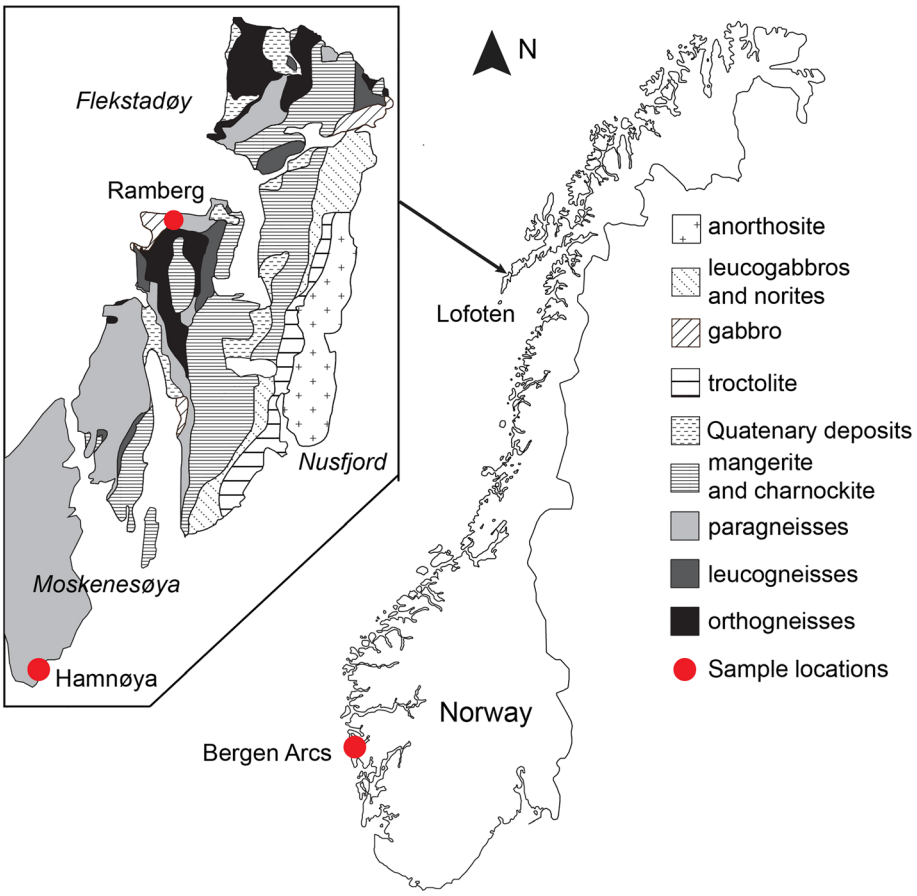

Figure 1. Schematic drawing of Norway showing the different sample locations in the Bergen Arcs, SW Norway, and in the geological map (Griffin et al., 1978; Steltenpohl et al., 2006) of the Lofoten Archipelago, Northern Norway.

mangerites rather than paragneisses. The other two samples were drilled from gabbronorite boulders exposed on a beach close to Ramberg (Figures 2b and 2c).

A mafic granulite was collected on Holsnøy in the Bergen Arcs, SW Norway (60°31′06.5″N 5°12′31.9″E; Figures 1 and 3) to serve as starting material for the deformation experiments. We preferred the Holsnøy sample over the Lofoten samples for the experiments, because it (i) shows a more homogeneous mineralogy with ~94 wt.% plagioclase (Figure 3; Table 1), which (ii) reveals very little hydration evidenced by the purplish color (Figure 3), and (ii) shows a plagioclase composition that is almost the average of the plagioclase analyses of the Lofoten samples (Figure 4; Table 1). However, our scanning electron microscope (SEM) studies reveal that the sample contains minor epidote needles and hence a small amount of structurally bound water (Figure 3). However, epidote is stable at the experimental conditions and will therefore not liberate fluids due to dehydration.

Table 1
Representative Plagioclase Analyses of the Three Different Sampling Locations

Oxide	Plagioclase experiments (Holsnøy)	Hamnøya plagioclase	Ramberg plagioclase core	Ramberg plagioclase rim
SiO_2	54.55	59.46	57.01	51.48
Al_2O_3	28.09	25.30	26.73	30.44
CaO	10.76	7.38	8.89	13.3
Na_2O	5.32	7.59	6.78	3.87
K_2O	0.22	0.24	0.09	0.05
Total	98.94	99.97	99.5	99.14
	An47Ab52Or1	An35Ab64Or1	An42Ab58	An65Ab34

4. Experimental and Analytical Methods

4.1. Experimental Methods

In total, eight deformation experiments were conducted using a Griggs-type apparatus (Moghadam et al., 2010; Rybacki et al., 1998). Four "as-is" samples and four samples with ~1 wt.% added water were deformed at either 700°C or 900°C and to either ~7% to 8% or ~33% to 36% axial strain to test the influence of water and temperature as well as to document the microstructural evolution (Table 2). All experiments were performed at a confining pressure ($P_c = \sigma_3$) of 2.5 GPa, that is, eclogite-facies conditions, and at a constant strain rate of ~5×10^{-5} s^{-1} (Table 2).

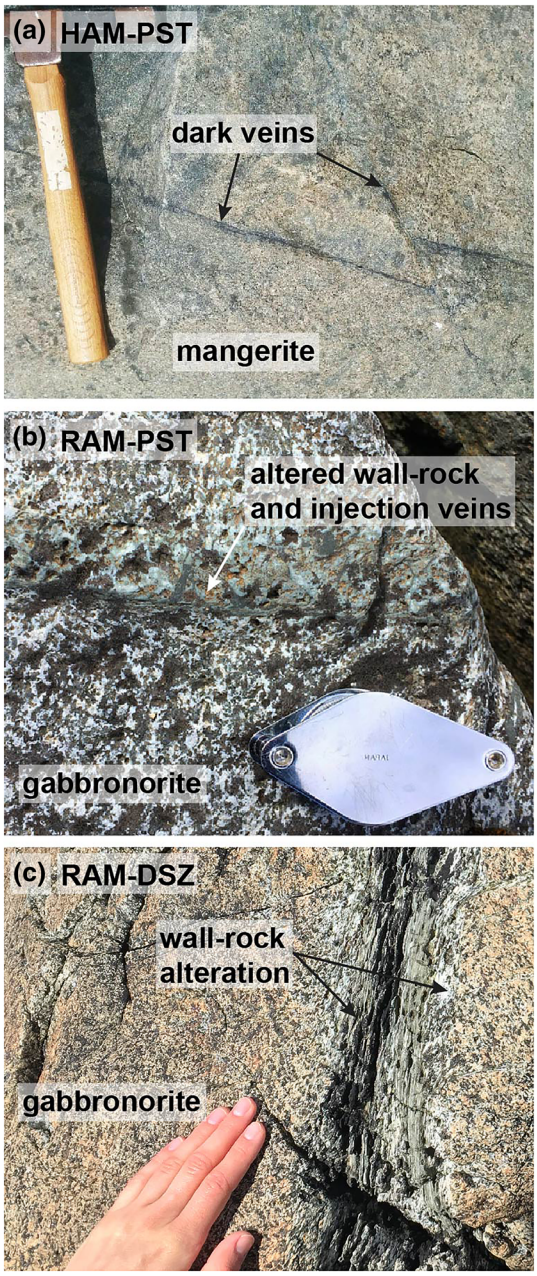

Figure 2. The natural samples used for this study. (a) The sample HAM-PST was collected close to the village Hamnøya. The outcropping rock is an orthogneiss revealing numerous dark veins. (b) Gabbronorite boulder exposed on the beach close to Ramberg, Lofoten Islands. This boulder shows a narrow intensely sheared zone with wall-rock alteration (greenish color) on only one side. Sample RAM-PST was drilled out of this boulder. (c) Centimeter-wide shear zone showing symmetric wall-rock alteration (whitish color) in a gabbronorite boulder located on the beach close to Ramberg. Sample RAM-DSZ was drilled out of this boulder.

4.1.1. Starting Material and Sample Preparation

The mafic granulite sample from Holsnøy shows plagioclase grains ranging between ~0.5 and 3 mm that make up ~94 wt.% (Figure 3). Garnet, pyroxene, spinel, corundum, alkali-feldspar, epidote, dark mica, and quartz constitute the remaining 6 wt.%. We drilled cores with a diameter of ~3.5 mm that were cut and polished to a height of ~8 mm. Hence, the feldspar grains have diameters similar to the sample diameter. Experimental studies on the rheology of rocks use intact rocks or synthetic aggregates with grains that are 2 to 3 orders of magnitudes smaller than the actual sample size to ensure that the sample volume constitutes a statistically representative volume. The present study, however, did not intend to quantitatively constrain the rheological behavior of plagioclase-rich rocks at elevated pressure and temperature conditions, as extensively studied in the past (Rybacki et al., 2006; Rybacki & Dresen, 2000, 2004; Stünitz et al., 2003; Stünitz & Tullis, 2001; Tullis & Yund, 1985, 1987, 1992). Previous experiments on fine-grained plagioclase-rich rocks revealed brittle deformation, for example, grain-scale faulting and microcracking, at 1.5 GPa and at temperatures up to 700°C, yet the deformation remained fully distributed throughout the samples even after axial shortening by 30% to 40% (Tullis & Yund, 1992). Using samples that contain grains with diameters that are almost equal to the sample's diameter was beneficial for this study, because this increased the chances for strain localization on the sample scale by faulting along grain boundaries and cleavage planes of plagioclase that act as laboratory analogs for strain localization in narrow zones in nature, that is, pseudotachylytes.

For the four runs on "as-is" samples, the drill cores were placed into a gold capsule without further treatment. We assume that the "as-is" samples exhibit water contents of ~0.2 wt.% H_2O (Bhowany et al., 2017). For the other four runs, we added ~20 μl of distilled water, corresponding to ~1 wt.%, into the gold capsule surrounding the drill-core sample. The capsules were sealed by placing a gold foil with a thickness of ~0.23 mm and an alumina piston with a thickness of ~1 mm on top of the drill-core sample. Since we do not weld the capsules, some water may escape during syncompressional heating. The confining medium used for the experiments was NaCl.

After an experiment, the recovered sample was axially cut into halves. For the chemical and microstructural investigations, one sample half was conserved in epoxy and polished. Additionally, thin sections were prepared from three selected experimental runs using the other sample halves as well as from the four natural samples.

4.1.2. Experimental Procedure

Every experiment involved three stages, which are pressurization and heating, isothermal deformation, and cooling and decompression. During the first stage, pressure and temperature were increased at 1 MPa/min and 10°C/min, respectively. After the required confining pressure and temperature were reached, deformation commenced by advancing the deformation piston with a velocity of 1.5 mm/hr. Once the required axial strain was achieved, we retracted the deformation piston with 1.5 mm/hr and decompressed the assembly with 1 MPa/min and initialized cooling at 10°C/min.

4.2. Analytical Methods

Microstructural investigations of the samples were performed using a polarized light microscope and a Hitachi SU5000 field-emission SEM (FE-SEM) for thin sections and carbon-coated polished slabs,

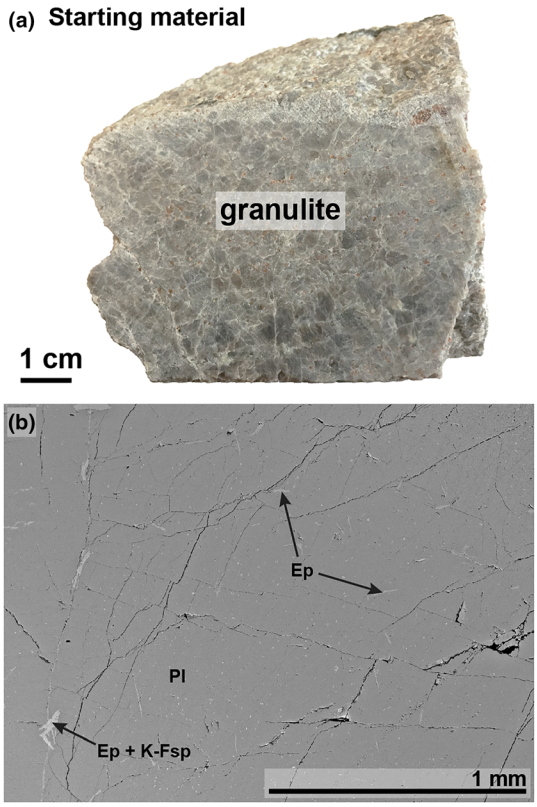

Figure 3. The sample used as starting material for the deformation experiments. (a) The hand specimen was collected on Holsnøy in the Bergen Arcs, SW Norway. This sample mainly comprises of purple plagioclase (Pl) and minor garnets. (b) A BSE image shows that this rock also contains some epidote (Ep) intergrown with alkali-feldspar (K-Fsp).

respectively. Chemical analyses were obtained on the slabs using a Cameca SX100 electron microprobe (EMP). The acceleration voltage was 15 kV at the SEM and the EMP. The phases present in the natural samples as well as in the recovered deformation samples were identified using energy-dispersive spectroscopy (EDS) at the SEM together with additional chemical analyses at the EMP.

5. Results

5.1. Microstructures of the Lofoten Samples

All the natural samples collected on the Lofoten all show evidence for strain localization (Figure 2). In the Hamnøya sample, referred to as HAM-PST in the following, strain is localized in narrow millimeter-thick zones forming a network of dark veins offsetting each other (Figure 2a). The Ramberg samples, RAM-PST and RAM-DSZ, also reveal strain localization, but in these two samples, deformation seems to be accommodated in centimeter-thick zones showing either asymmetric (RAM-PST) or symmetric wall-rock alteration (RAM-DSZ; Figures 2b and 2c).

A scan of the HAM-PST thin section reveals several narrow veins that appear almost black in a host rock of mainly colorless and transparent grains (Figure 5). Semiquantitative and quantitative chemical analyses by the SEM and the EMP show that the host rock contains dominantly alkali-feldspar and plagioclase ($anorthite_{35}albite_{64}orthoclase_1$, Figure 4; Table 1). Minor phases are orthopyroxene ($enstatite_{75}ferrosilite_{21}$), Ti-magnetite, and apatite. In crossed polarized light, plagioclase, alkali-feldspar, and quartz crystals exhibit undulatory extinction, and some plagioclase grains reveal mechanical twins in close vicinity to the dark veins (red arrows in Figure 5b). The dark veins are composed of wall-rock fragments within a matrix of alkali-feldspar, plagioclase, and orthopyroxene showing a rather homogeneous grain size ~10–50 μm, that is, significantly smaller than the grain size in the host rock. Additional phases present in the dark veins are small sulfide spheres, appearing bright in the backscattered-electron (BSE) images (Figures 5b and 5c), and garnet crystals, exhibiting a cauliflower-shape owing to numerous inclusions, indicative of rapid growth (Figure 5c). Furthermore, we find a feature resembling an injection vein oriented normal to the main vein (Figure 5c). The combination of wall-rock fragments, cauliflower garnets, sulfide spheres, and an injection vein lets us interpret the narrow dark veins as pseudotachylytes (Kirkpatrick & Rowe, 2013). Except for the occurrence of the sulfide spheres and minor amounts of amphibole, formed by orthopyroxene hydration, the mineral assemblage of the pseudotachylyte veins is similar to that of the host rock. Yet, in the pseudotachylyte, orthopyroxene and plagioclase are slightly richer in Fe ($enstatite_{70}ferrosilite_{25}$) and Na ($anorthite_{30}albite_{70}$), respectively, than in the host rock. We do not observe any alteration of the wall rock adjacent to the pseudotachylyte, and the contacts between pseudotachylyte and wall rock are sharp.

In contrast to the Hamnøya host rock, the host rock of the RAM-PST sample consists dominantly of plagioclase with minor clinopyroxene and orthopyroxene, but also some hydrous phases such as biotite and amphibole, with the latter being present as polycrystalline rims surrounding pyroxene crystals (Figure 6). Locally, garnets grew between the amphibole rim and the plagioclase matrix (Figures 6b and 6c). A 0.5–0.8 mm thick vein contains mainly plagioclase, amphibole, and cauliflower garnet that all exhibit grain sizes in the range of ~10 to 20 μm. Because this vein exhibits the same characteristics as the previously described pseudotachylyte veins in the HAM-PST sample, for example, host rock fragments, cauliflower garnets, and sulfide spheres (Figures 6b and 6c), we will refer to it as a pseudotachylyte vein as well. The appearance of the pseudotachylyte borders to the adjacent wall rock varies from sharp to diffuse on the thin-section scale (Figure 6a). Adjacent to the pseudotachylyte vein, only the upper part of the wall rock appears to be extensively sheared and chemically altered, highlighted by the greenish color (Figure 6). In contrast to the lower part that contains minor amounts of amphibole, occurring as rims around pyroxene, the upper part reveals

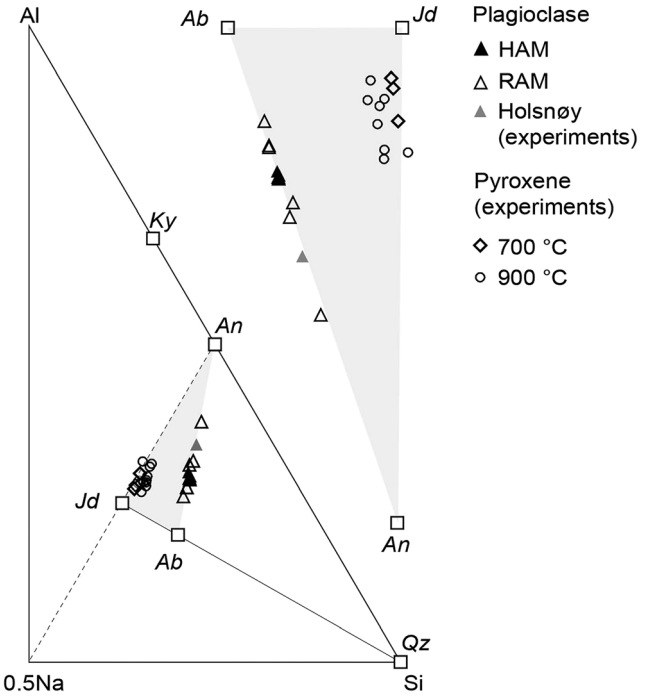

Figure 4. Al-Si-0.5Na ternary diagram showing the chemical composition of the different plagioclase compositions of the Hamnøya (HAM), the Ramberg (RAM), and the Holsnøy sample that was used for the experiments. Additionally, it shows the chemical composition of the newly formed pyroxenes that were measured in the experimental samples in an albite (Ab)-jadeite (Jd)-anorthite (An) diagram. Ky, kyanite; Qz, quartz.

abundant amphibole as a matrix phase—especially within 2 to 3 mm distance from the pseudotachylyte vein. The amphibole is a pargasitic hornblende and reveals no significant variation in composition at the thin-section scale. Furthermore, a structure resembling a sheared injection vein appears in the altered and sheared upper part of the thin section (Figure 6a).

A first main difference between the pseudotachylytes in the HAM-PST and the RAM-PST samples is the abundance of amphibole in the latter, reflecting hydration (Figure 6). A second difference is that the HAM-PST sample shows sharp borders between the pseudotachylyte vein and the adjacent wall rock while the RAM-PST sample reveals extensive shearing and wall-rock alteration, including hydration of clinopyroxene and replacement by amphibole. The replacement is especially pronounced on one side of the pseudotachylyte (upper part of Figure 6b), giving it a more greenish color relative to the opposite side that mainly contains plagioclase (lower part of Figure 6b).

The RAM-DSZ sample shows a shear zone with a width of ~4 cm that comprises a central, intensely sheared, greenish zone with a thickness of ~0.5 mm (Figure 7) and a surrounding zone characterized by whitish altered wall rock with a significant planar fabric, mostly expressed by fine-grained plagioclase crystals (grayish colors) flowing around host rock pyroxenes and micas (colored crystals; Figures 7b–7d). Feldspar crystals located several millimeters away from the central shear zone reveal some mechanical twinning or undulatory extinction (Figure 7d). The central shear zone consists mostly of plagioclase and amphibole in equal amounts as well as some clinopyroxene and cauliflower garnets. All phases show grain sizes ranging from ~10 to 50 μm. Sulfide spheres are far less abundant than in the pseudotachylytes of the HAM-PST and RAM-PST samples. The main difference between the microstructures of the HAM-PST and that of the RAM-PST and the RAM-DSZ samples is the width of the zone that accommodated deformation and the larger amount of hydrous phases in the latter, such as amphibole, indicating extensive hydration.

5.2. Laboratory Experiments

5.2.1. Mechanical Data

Irrespective of water treatment or temperature, peak stress was reached at approximately 8–11% axial strain (Figure 8). The runs conducted at 700°C show consistently higher strengths than those performed at 900°C except for the high-strain, "as-is" sample deformed at 700°C that exhibits a lower strength than either its low-strain counterpart or the sample deformed "as-is" at 900°C (Figure 8a). The "as-is" samples show a sequence of post-peak weakening and restrengthening in the runs conducted at 700°C and steady-state flow when deformed at 900°C (Figure 8a). The samples with water added that were shortened to over 30% strain exhibit extensive post-peak weakening (Figure 8b). Comparing the peak-stress values between the low-strain and the high-strain runs reveals that the tests with water added show a reproducibility within ±50 MPa, whereas samples deformed "as-is" exhibit variability in strength of ~150 to 300 MPa (Figure 8).

Table 2
Experimental Conditions of the Eight Deformation Tests

Comment	T (°C)	Total axial strain (%)
"as-is"	700	7
"as-is"	700	36
"as-is"	900	7
"as-is"	900	35
+1 wt. H_2O	700	8
+1 wt. H_2O	700	33
+1 wt. H_2O	900	8
+1 wt. H_2O	900	36

Note. Every experiment was deformed at a confining pressure of ~2.5 GPa and at a strain rate of approximately 5×10^{-5} s^{-1}.

5.2.2. Microstructural Analysis

5.2.2.1. Samples Deformed "As-Is"

The two samples deformed at 700°C either to peak-stress conditions (~7% strain) or to ~36% axial strain exhibit brittle faults in BSE mode (Figures 9a–9d). The faults displace epidote crystals (Figures 9a–9d). The low-strain sample shows no fault gouge, whereas the faults in the high-strain sample are filled with mostly plagioclase fragments. At high magnification, the fault borders and the adjacent wall rock of the

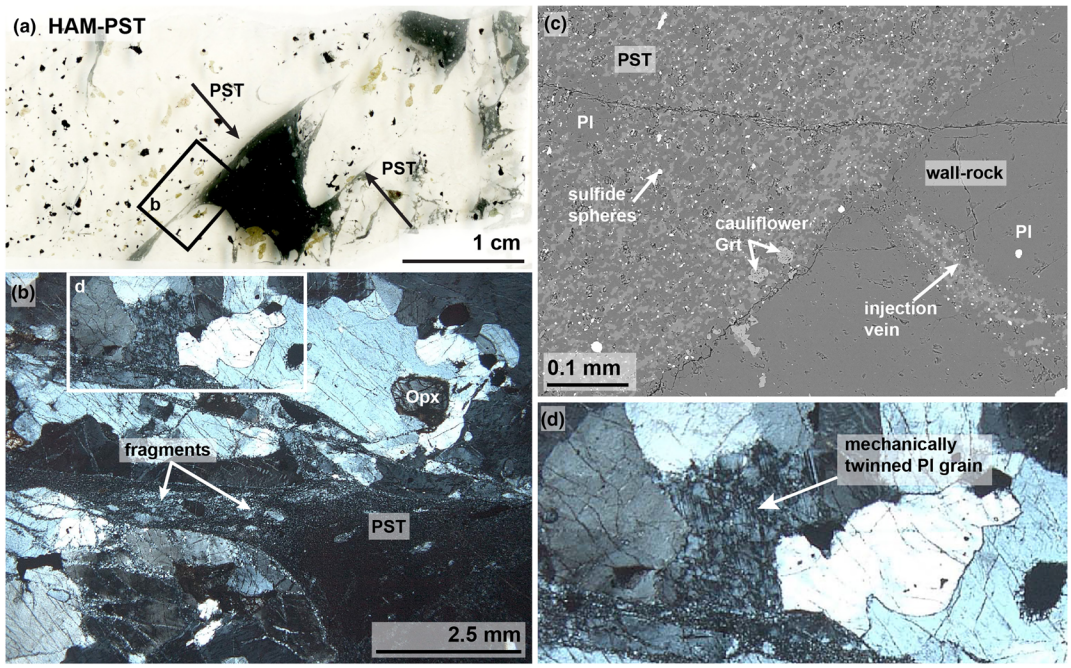

Figure 5. (a) Scan of the thin section made of the HAM-PST hand specimen exhibiting two parallel pseudotachylyte (PST)-bearing faults. The host rock is comprised by plagioclase, alkali-feldspar, quartz, and minor orthopyroxene (brown grains) and Ti-magnetite (black grains). (b) Microphotograph taken under cross-polarized light. The pseudotachylyte appears very dark and incorporates wall-rock fragments. Adjacent wall-rock plagioclase grains show extensive mechanical twinning (white arrows) and undulatory extinction (mostly alkali-feldspar and quartz). (c) BSE image revealing that the pseudotachylyte is completely recrystallized to plagioclase (Pl), alkali-feldspar (K-Fsp), and orthopyroxene (Opx). Rare garnets (Grt) and tiny (<1 m) sulfide spheres are homogeneously distributed throughout the pseudotachylyte-matrix. An injection vein oriented perpendicular to the main vein is seen in the lower right corner. (d) Mechanically twinned wall-rock plagioclase next to a pseudotachylyte vein.

high-strain sample are decorated with needle-shaped grains identified as zoisite (Figure 9d). The reacted plagioclase volume of the recovered samples was estimated by visual inspection of the samples in the SEM. Evidence for the onset of eclogite-facies reactions is absent in the low-strain sample. The high-strain sample locally exhibits the growth of zoisite, but the overall reacted plagioclase volume is estimated to be <1 vol.%.

In polarized light, the high-strain sample deformed at 900°C shows conjugated faults, cutting through several grains, microcracking of the wall-rock plagioclase, and extensive mechanical twinning under crossed polarized light (Figures 10a and 10b). Microcracks seem to have predominantly formed along twins and cleavage planes. Since their orientation seems to be controlled by the plagioclase crystallography, microcracks are often arranged in sets of parallel cracks exhibiting the same orientation (Figure 10a). In BSE mode, both low- and high-strain samples deformed at 900°C reveal that reaction preferentially took place on one side of the faults (Figures 9e–9h). Yet, sections with one-sided reaction appear to shift the side of the fracture.

The low-strain sample exhibits newly formed zoisite crystals that appear brighter and jadeite crystals that appear darker than the plagioclase matrix in BSE mode (Figures 4, 9e and 9f). Zoisite shows a range in grain size from ~1 to 20 μm; the largest grains exhibit tabular crystal shapes. Jadeite crystals are subhedral to euhedral with sizes from ~10 to 20 μm (Figures 9e and 9f). The high-strain sample shows anhedral quartz crystals, mostly situated in the faults (Figure 9h) in addition to zoisite and jadeite. The grain size of the newly formed phases, that is, zoisite, jadeite, and quartz, in the high-strain sample is ~1 to 10 μm and thus slightly smaller than the grain size of these product phases in the low-strain sample (~1–20 μm; Figures 9e–9h). Zoisite appears needle-like, while jadeite crystals are either rounded or lenticular. The elongated shapes seem to go along with a "bimodal" shape-preferred orientation with zoisite needles and jadeite lenses oriented either parallel or perpendicular to the fault (Figure 9h). The reacted plagioclase volume was estimated to be ~1 and <5 vol.% for the low- and high-strain samples deformed "as-is" at 900°C, respectively. Thus, both show a higher reaction progress than the samples deformed "as-is" at 700°C.

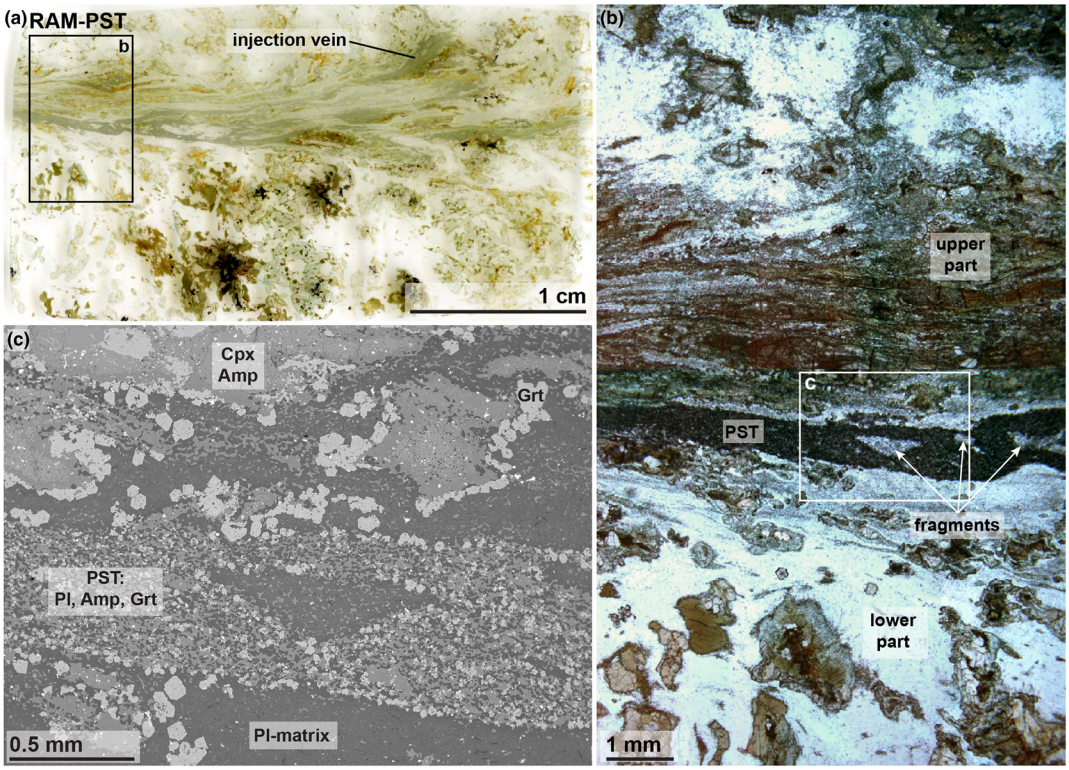

Figure 6. (a) Scan of the RAM-PST thin section showing extensive shearing and alteration of the upper part of this section. The black rectangle marks the position of the microphotograph shown in panel (b). (b) In polarized light, bright areas are mainly composed of plagioclase. The brownish-greenish crystals in the host rock are orthopyroxene and dark mica. The central part of this image shows a pseudotachylyte (PST) incorporating host rock fragments. The upper part is extensively sheared. The lower part of the PST reveals less shearing and alteration. (c) BSE image showing the pseudotachylyte and its vicinity. The pseudotachylyte is recrystallized and mainly consists of plagioclase (Pl), amphibole (Amp), and dendritic garnet (Grt) as well as homogeneously distributed sulfide spheres. The mostly unaltered host rock, represented by the lower part, is composed of plagioclase (Pl-matrix), orthopyroxene that shows coronas mainly of amphibole, and dark mica. The upper part of the pseudotachylyte reveals abundant amphibole indicating hydration.

5.2.2.2. Samples Deformed With Water Added

In polarized light, the high-strain sample deformed at 700°C reveals slip along faults. Areas consisting of grains much smaller than the initial plagioclase grains are often found right next to the faults that accommodated slip and appear dark (Figures 10c and 10d). In the SEM, these fine-grained zones were identified as the reaction products zoisite and jadeite together with minor quartz and occasionally muscovite. Strikingly, the wall-rock reaction preferentially took place on one side of the faults but was not restricted to the same side (Figures 10b and 11a–11d). The grain size of the reaction products of the samples deformed at 700°C decreases with strain from ~10 to 50 μm at 8% to ~1 to 20 μm at 36% with very few zoisite grains larger than 20 μm (Figures 11a–11d). The low-strain sample shows less reacted plagioclase relative to its high-strain counterpart. Reacted plagioclase volumes were estimated to be ~5 and 20 vol.%, respectively.

After deformation at 900°C with water added, the low-strain sample reveals faults, the majority of which show wall-rock alteration on one side (Figures 11e and 11f). The reaction products are zoisite and jadeite and some minor quartz. Their grain size ranges from 10 to 30 μm (Figure 11f), and the reacted plagioclase volume was estimated to be <10 vol.%. The high-strain sample demonstrates structures that appear more like ductile shear zones than faults (Figures 10e, 10f, 11g, and 11h), showing symmetrical wall-rock reaction and shearing across a central zone that is only <10 μm wide. We estimate that ~60 vol.% of the initial sample was replaced by zoisite, jadeite, quartz, and occasionally muscovite. Since most of the initial plagioclase reacted, we do not observe unequivocal evidence for brittle deformation of plagioclase, for example, grain-scale faulting and microcracking. The grain size of the reaction products is not uniform on the two sides of the fault, however, with one side showing grains of ~1 to 10 μm and ~5 to 20 μm on the opposite side (Figures 11g and 11h).

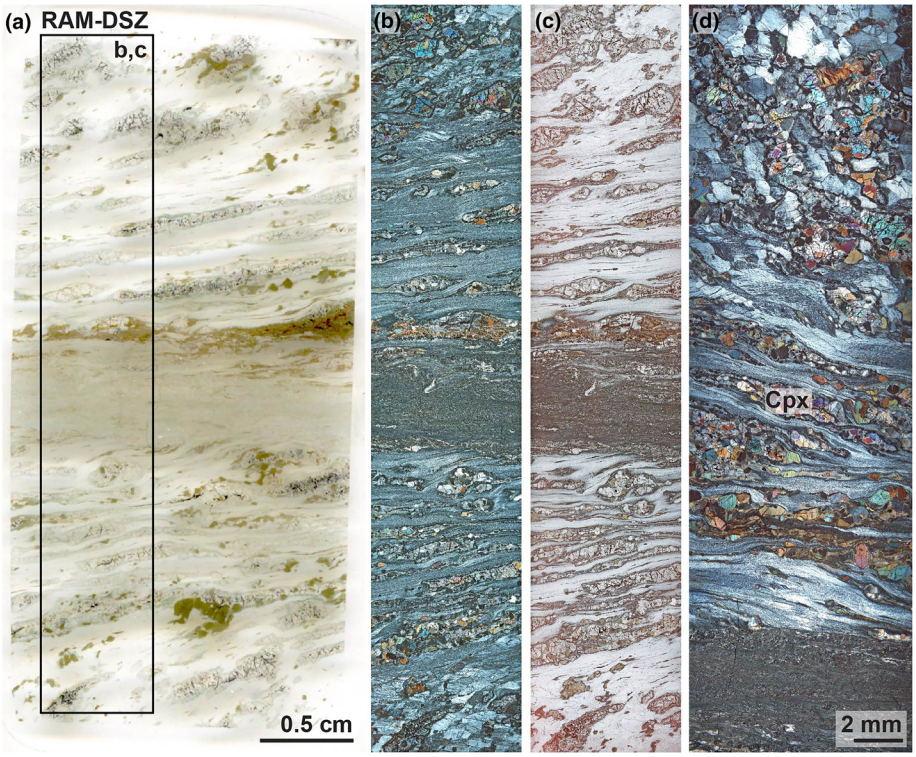

Figure 7. (a) Scan of the RAM-DSZ sample with black rectangle highlighting the higher magnification images shown in panels (b) and (c). The host rock mineral assemblage is the same as for the RAM-PST sample but reveals abundant amphibole. The central part of this section shows an approx. 0.5 cm wide central shear zone that appears greenish. (b and c) Image taken with (b) and without (c) crossed polarizers. The grain size within the shear zone is much smaller compared to the host rock. Shearing of the wall rock is symmetric. (d) High magnification image taken with crossed polarizers.

6. Discussion

6.1. The Role of Water During Eclogitization of Granulites

Samples that underwent reaction reveal the growth of zoisite and jadeite, as well as quartz and occasionally muscovite in the samples with water added, confirming that deformation took place under eclogite-facies conditions (Goldsmith, 1980, 1981). Although thermodynamic equilibrium might not have been achieved due to the short run durations of ~25 or ~112 min for the low- and high-strain experiments, respectively, we calculated the stable mineral assemblage with associated mineral amounts using PerpleX for comparison with the experimental results (Connolly, 1990). For the "as-is" samples, we observe the growth of zoisite and jadeite in almost equal proportions (Figures 9e–9h). This is a considerably lower jadeite/zoisite ratio than the calculated value (≈3.6) for an initial water content of ~0.2 wt.% H_2O (Table 3). Thermodynamic modeling shows that muscovite is stable at water contents >0.75 wt.%. The absence of muscovite in the "as-is" high-strain sample deformed at 900°C and the presence in its water-added counterpart supports our inference on the significantly different water contents of the two sample types. At water contents of 1 wt.%, the calculated mineral assemblage fits well with the experimental results for the samples with water added (Table 3). The other phases expected from thermodynamic modeling, notably kyanite and garnet, were not observed neither in the "as-is" nor in the water added samples, because they probably failed to nucleate or grow.

Samples deformed at 700°C show less reacted plagioclase relative to their 900°C counterparts, and samples deformed with added water all exhibit a higher volume of reacted plagioclase than the samples deformed "as-is." The difference in volume of reacted plagioclase can be explained by the dependence of reaction kinetics on temperature and water with higher reaction rates at higher temperatures in the presence of water.

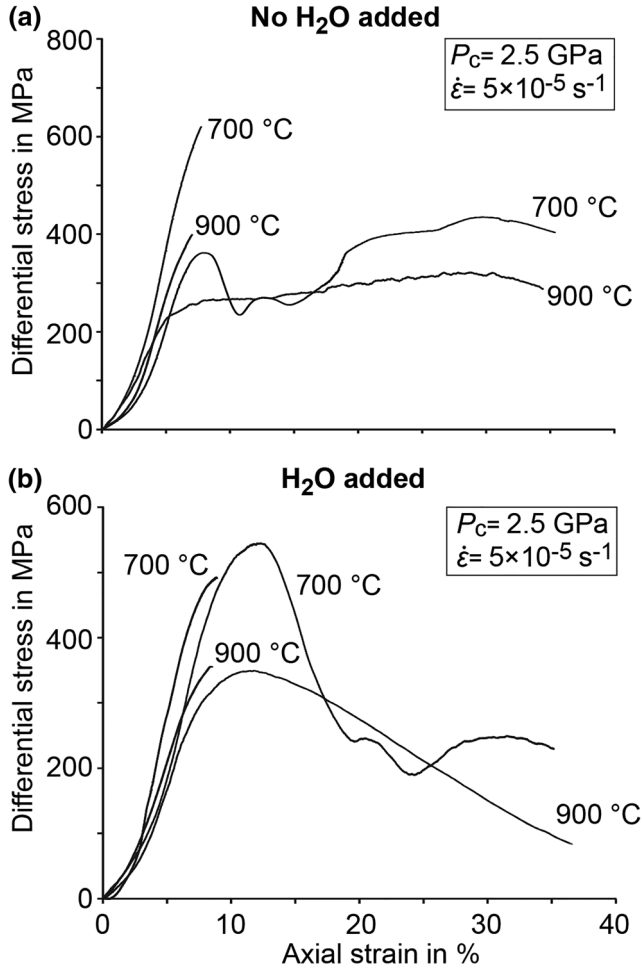

Figure 8. Stress-strain curves of the eight deformation experiments. (a) Four experiments deformed "as-is" without additional water. The low-strain runs were stopped at around 7% axial strain and the high-strain tests at approx. 35%. (b) Stress-strain curves for samples deformed with added water (around 1 wt. %). The four runs show a uniformly lower strength than their "as-is" counterparts, and the high-strain tests show extensive weakening toward the end of the experiment at ~33 to 36% axial strain.

6.2. Impact of Grain Size and Plagioclase Cleavage on the Mechanical Behavior

The range in strength of ~250 to 630 MPa observed for our "as-is" samples (Figure 8) falls below the strength of ~1.5 GPa, previously reported for plagioclase-rich rocks deformed at comparable conditions (Stünitz & Tullis, 2001; Tullis & Yund, 1992). The strength discrepancy might be due to the larger average grain size (approximately 1 mm) in our samples relative to the average grain sizes of ~0.5 mm and <10 μm for the starting materials used by Tullis and Yund (1992) and Stünitz and Tullis (2001), respectively. For brittle failure, grain size and strength correlate inversely (Brace, 1961; Fredrich et al., 1990). A previous study on the deformation of plagioclase single crystals at high-pressure, high-temperature conditions shows a range in strength of ~200 to 800 MPa depending on the orientation of the two perfect cleavage planes of plagioclase relative to the direction of maximum compression (Stünitz et al., 2003). Our sample strengths fall well within this range, and the microstructures also reveal slip along plagioclase-cleavage planes which may influence the sample strength, as documented by Stünitz et al. (2003) on plagioclase single crystals (Figures 10c and 10d). Thus, the dependence of plagioclase crystal orientation on sample strength may explain the sample-to-sample variability in our deformation experiments (Figure 8). Experiments using natural drill cores in which the presence of minor phases, for example, garnet, spinel, and corundum, may differ from sample to sample may also add to the variability in overall sample strength. A further indicator that our samples' failure behavior resembles that of single crystals rather than of polycrystalline aggregates is the occurrence of microcracks in most of our samples, although maximum differential stresses (σ_1–σ_3) all fell well below the Goetze criterion (σ_1–$\sigma_3 = \sigma_3$; Figure 8). In general, the Goetze criterion is used as a threshold separating mainly semibrittle from fully plastic deformation behavior of polycrystalline samples but does not hold for the deformation of single crystals.

6.3. Link Between Deformation and Reaction of Plagioclase

The microstructural observations of the experimentally deformed samples demonstrate that plagioclase grains are less deformed in samples with added water relative to samples deformed "as-is," which reveal extensive mechanical twinning and associated microcracking as well as grain-scale faulting and slip along cleavage planes (Figures 9 and 10a). The absence of extensive plagioclase deformation in the high-strain samples deformed with water added demonstrates that strain must have been accommodated almost exclusively in the zones that underwent transformation to eclogite-facies minerals.

Rocks that undergo syndeformational reactions may show "transformation plasticity," which refers to bulk weakening by localization of strain in reacted volumes (Poirier, 1982). The extensive post-peak stress weakening of the highly reacted samples suggests that the reacted volumes are indeed weaker than the initial plagioclase (Figure 8b). Weakening of plagioclase-rich samples undergoing metamorphic reactions has also been documented for deformation experiments at amphibole-facies conditions (Mansard et al., 2020). When reactions are involved, the deformation behavior of the bulk sample will depend on the relation between reaction and deformation rate (Burnley et al., 1991; Incel et al., 2019). Recently, it has been experimentally demonstrated that samples that react fast relative to the imposed strain rate are weak and ductile, whereas brittle mechanisms dominate in the absence of reactions (Incel et al., 2019). In the current experiments, we applied a fixed deformation rate but aimed to vary reaction rate by varying temperature and the availability of water. While ongoing reaction has first-order effects on the deformation of some samples (e.g., sample deformed with water added at 900°C), the mode of deformation in others is mainly controlled by the

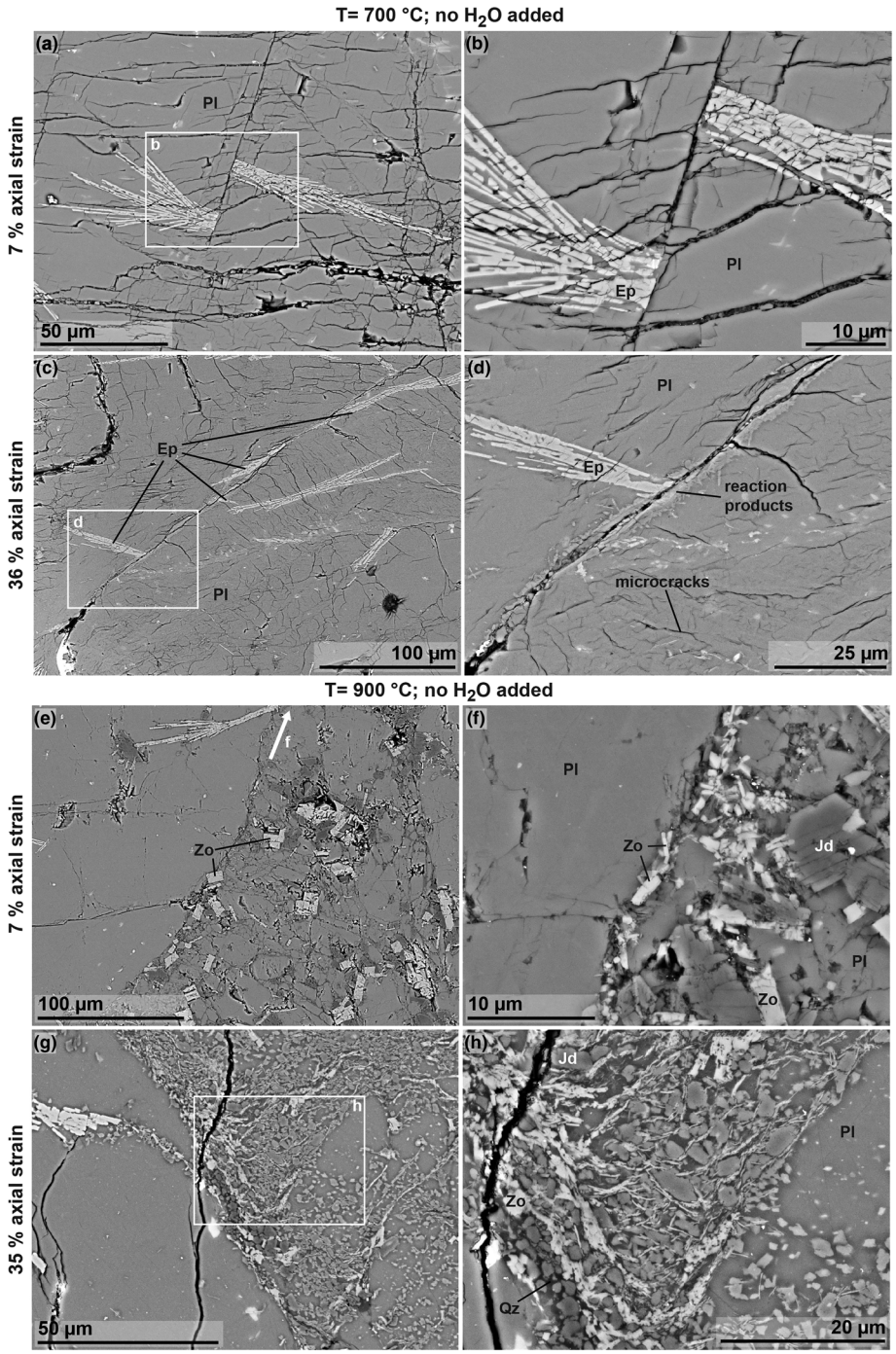

Figure 9. BSE images of the experimental samples deformed as-is. The direction of maximum compression (σ_1) is oriented perpendicular to the longer edge of the images. (a and b) Two BSE images of the low-strain (~7% axial strain), low-temperature (700°C) sample, showing the same area taken at different magnifications. A sharp fault dissected and displaced a bundle of preexisting epidote needles. The fault reveals no fault gouge and no evidence for reaction within the wall-rock plagioclase (Pl). (c and d) Microstructures formed at the same temperature conditions but after around 36% axial strain. There are more microcracks present in the wall rock relative to the low-strain sample. Some fracture margins are decorated with small zoisite grains. (e and f) Sample deformed at 900°C until 7% axial strain shows faults that often reveal one side being more fractured and reacted (right hand side of the fracture) as expressed by the growth of zoisite (Zo) and jadeite (Jd). (g and h) Sample deformed at 900°C until 35% axial strain. Similarly to the low-strain sample, it also shows more reaction on one side. Reaction products are uniformly smaller than the newly formed grains in the low-strain sample and also demonstrate a shape preferred orientation. Minor quartz (Qz) occurs as a reaction product.

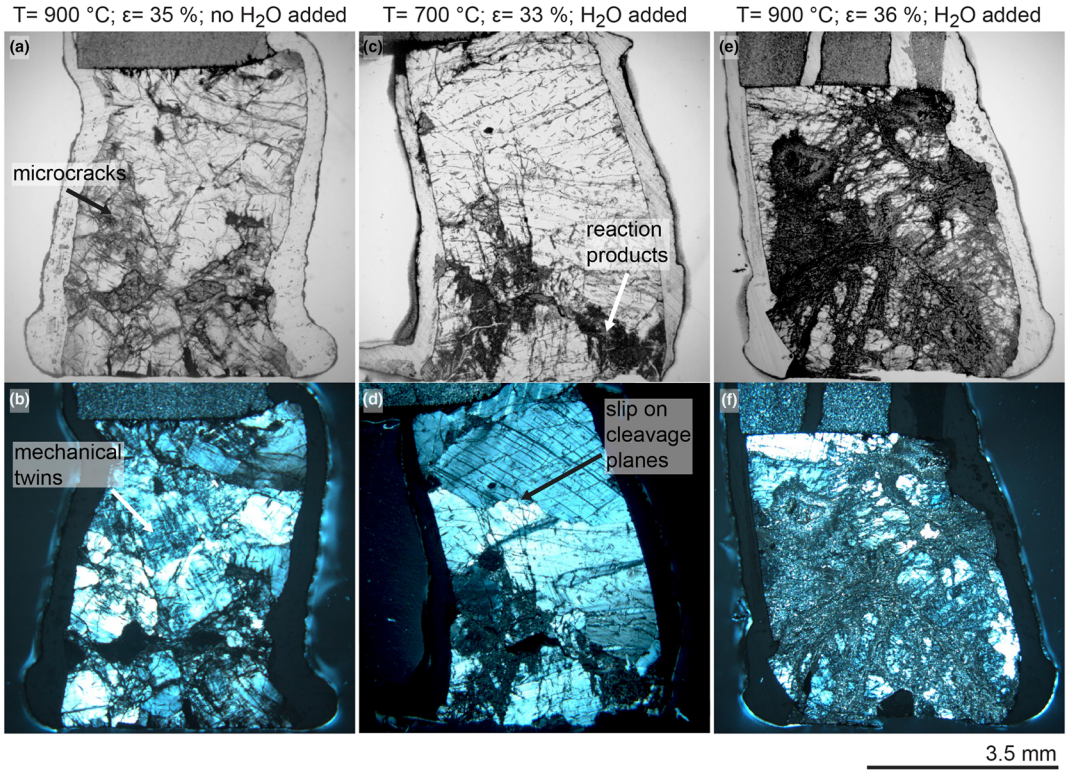

Figure 10. Three representative high-strain samples after deformation. The direction of maximum compression (σ_1) is always perpendicular to the upper/bottom edges of the images. Microphotographs (a), (c), and (e) were taken without and (b), (d), and (f) with crossed polarizers. (a and b) Sample deformed "as-is" at 900°C. The sample reveals some grain-scale faulting and microcracks that appear slightly darker than the plagioclase matrix in polarized light. (b) Most plagioclase grains reveal extensive mechanical twinning and undulatory extinction. (c and d) Sample deformed with added water at 700°C. This sample shows conjugated faults in the lower part of the sample. The lowermost side of these faults appears to show more reacted plagioclase. The upper part of this sample shows slip along the cleavage of a larger plagioclase crystal. (e and f) Sample deformed with added water at 900°C. This sample is covered with conjugated bands showing extensive transformation.

rheological behavior of the host rock (e.g., sample deformed "as-is" at 700°C). Regardless of the experimental conditions, samples deformed to low strain exhibit brittle faulting (Figures 9a, 9b, 9e, 9f, 11a, 11b, 11e, and 11f). Reactions, which vary in extent with conditions, took place along the faults and in their immediate vicinity, indicating that the onset of faulting must have preceded reaction (Figure 10b). From comparison with its low-strain counterpart, we conclude that the ductile shear zones in the sample deformed to high strain at 900°C with water added nucleated on faults, which were successively overprinted by reaction and by deformation of the reaction products (Figures 10c, 11g, and 11h).

The nonuniform grain-size distribution across faults in the high-strain sample deformed at 900°C with water added constitutes further evidence for strain localization in volumes of reacted plagioclase (Figures 11g and 11h). One side of the plastically overprinted faults shows grains with an average diameter of ~10 μm, which is similar to the measured grain diameters of the reaction products of the low-strain samples (Figures 9f, 11b, and 11f), whereas grains on the opposite side have a smaller average grain diameter of approximately 5 μm (Figures 11g and 11h). We interpret this difference in average grain size as an indicator of the succession of interrelated deformation and reaction. Fluid infiltration and associated reaction commences in plagioclase grains, adjacent to the fault that were favorably oriented in regard to mechanical twins, cleavage planes, and/or microcracks, which could be exploited as fluid pathways (Figure 12). The reaction, involving a negative volume change of approximately 14%, may reduce the local stresses, allowing the first reaction products to grow and transferring deformation to other sites, for example, the opposite side, where a second generation of reaction products forms. Meanwhile, the first generation of reaction products experienced grain size reduction by dynamic recrystallization due to ongoing compaction, leading to a distinct planar fabric (Figures 9h and 11h).

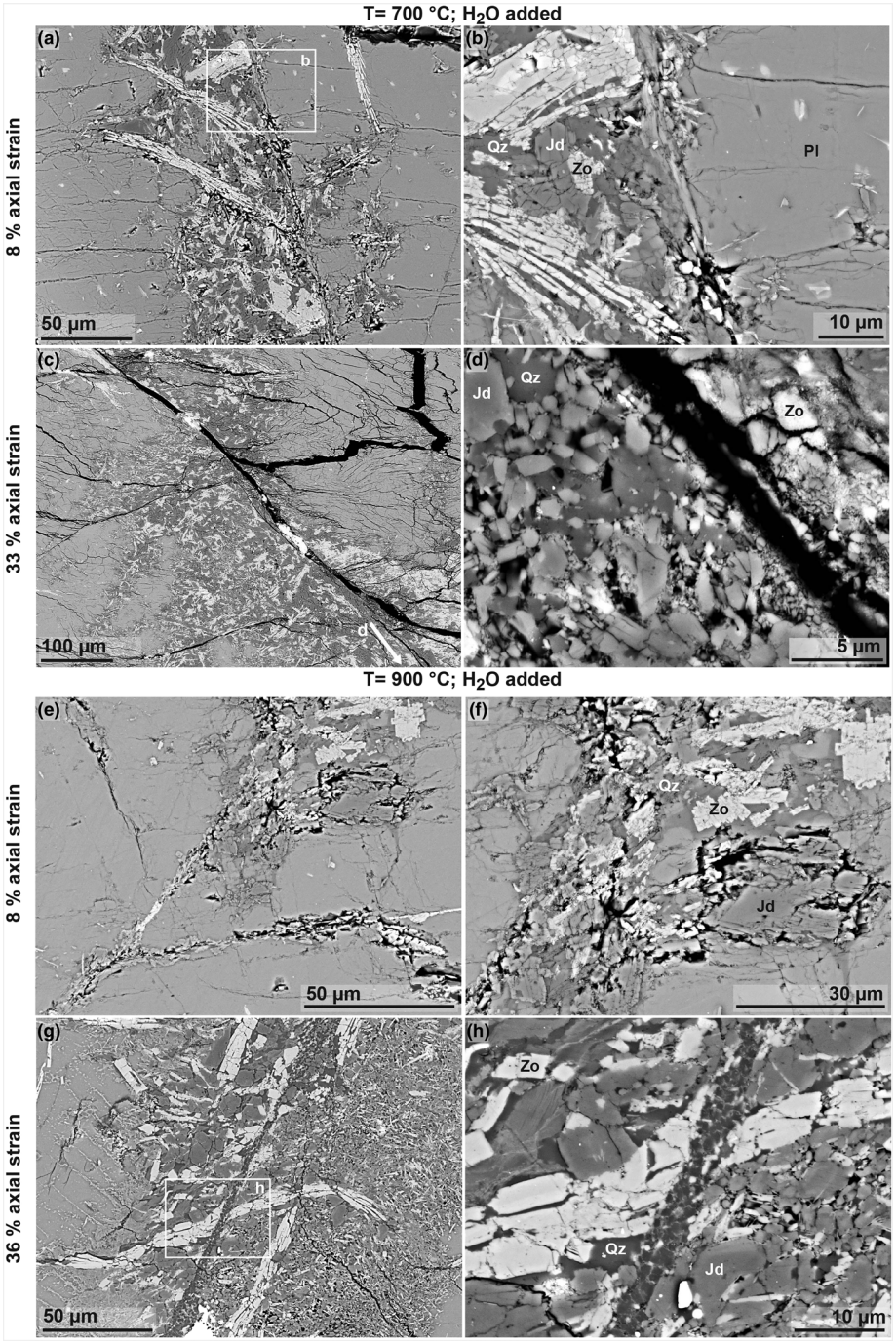

Figure 11. BSE images showing the microstructures of the four samples deformed with water added. The direction of maximum compression (σ_1) is oriented perpendicular to the longer edge of the images. (a and b) Microstructure of the low-strain sample deformed at 700°C. As in the "as-is" samples deformed at 900°C, there is much more reaction on one side of the faults. The new phases found on this side are zoisite (Zo), jadeite (Jd), and quartz (Qz). (c and d) Two images taken of the same area at different magnifications of the high-strain sample deformed at 700°C. A fault is still distinguishable with reaction taking place on mostly both sides. The grain-size of these newly-formed Zo, Jd, and Qz grains is consistently smaller relative to the average size of the crystals in the low-strain counterpart. (e and f) Microstructure of the low-strain sample deformed at 900°C. The sample shows more reaction on only one side of the fault. The grains are comparable in size to those of the low-strain 700°C sample. (g and h) The high-strain sample deformed at 900°C is the only sample that shows structures resembling conjugated ductile shear zones. In these shear zones, most of the initial plagioclase (Pl) reacted to form Zo, Jd, and Qz.

Table 3
Results of the Thermodynamic Calculations Assuming Three Different Water Contents in the Starting Material

At 700°C and 2.5 GPa		0.2 wt.% H_2O	0.75 wt.% H_2O	1 wt.% H_2O
Calculated amount in vol. %	Zoisite	9.08	36.87	37.37
	Jadeite	32.44	31.63	31.34
	Quartz	17.23	16.03	16.89
	Kyanite	14.83	6.89	4.74
	Garnet	19.51	1.82	1.73
	Sanidine	4.49	4.38	–
	Muscovite	–	–	5.65
	Sphene	0.23	0.23	–
	Diopside	2.19	2.14	1.88
	Rutile	–	–	0.08
	Glaucophane	–	–	0.32

Note. Because the phases present and their respective amounts in vol.% are not significantly different between 700°C and 900°C, we only present the results for 700°C and 2.5 GPa.

Combining the microstructural observations regarding the relation between faulting and reaction in the low-strain with the observation of reaction and strain localization in the high-strain samples, we postulate a sequence of events during deformation that comprises initial brittle faulting, enabling the influx of fluids into the interior of the sample, followed by reaction of plagioclase to zoisite, jadeite, and occasionally quartz and muscovite (Figures 9c–9h and 11). Depending on the amount of water present and the duration of an experiment, hydration and associated reaction result in a further widening of the plastically deforming zone from <1 μm to <50 μm for the "as-is" samples (Figures 9b and 9d) and from <1 μm to ~200 μm for the samples with water added (Figures 11b and 11h).

6.4. Evolution of Brittle Structures—Linking Laboratory Results and Natural Observations

While experimental deformation produces brittle features, it does not produce pseudotachylytes. However, natural shear fractures do not necessarily produce pseudotachylytes. The absence of pseudotachylyte-bearing faults in our experimental samples poses some problems when comparing the natural with the experimental microstructures. An additional challenge, when relating the laboratory results to nature, is the far more complex deformation history experienced by the natural samples in comparison to the experimental samples. Especially the two Ramberg samples, RAM-PST and RAM-DSZ, seem to

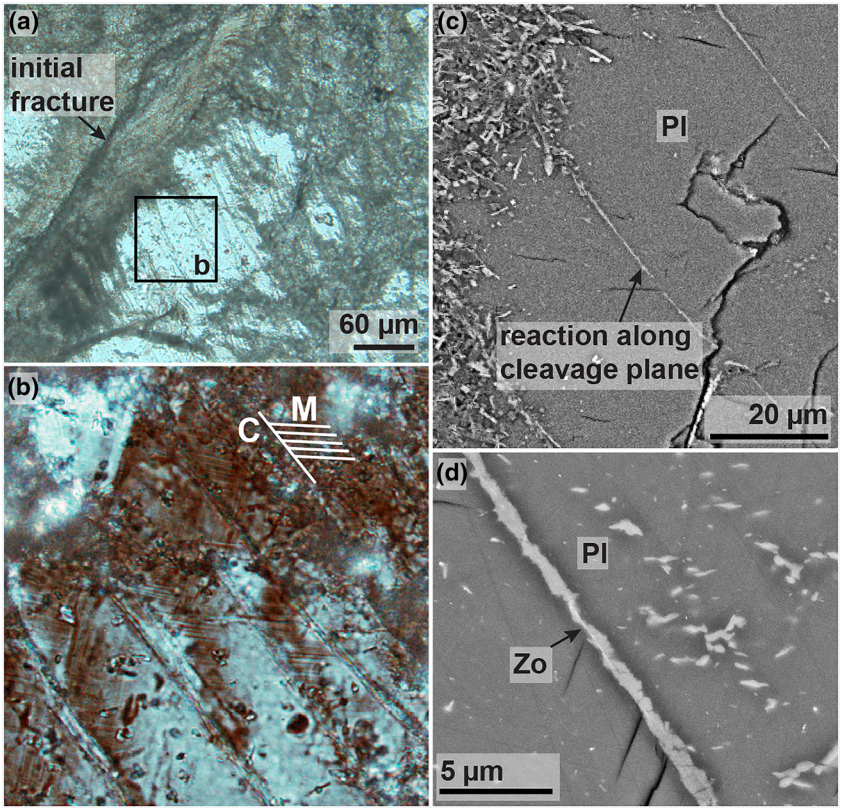

Figure 12. Hydration and reaction of the wall rock in the high-strain sample deformed with water added at 900 °C. (a and b) Micrographs taken at the polarized light microscope. (a) The initial fracture is completely overprinted by reaction and deformation of the reaction products. The black rectangle marks the position of the higher magnification image shown in panel (b). (b) Hydration occurs along cleavage planes. (c) Backscattered-electron image exhibiting fine zoisite needles along cleavage planes. (d) At higher magnification in the SEM, the microstructure reveals hydration along cleavage planes. Pl, plagioclase; Zo, zoisite; C, cleavage plane; M, mechanical twin.

have experienced alternating episodes of dominantly brittle or mainly plastic deformation. We speculate that the plastically deformed plagioclase matrix that is incorporated as fragments in the pseudotachylyte vein in the RAM-PST sample is evidence for an early cycle of first brittle deformation and subsequent plastic overprint (Figure 6c). In both Ramberg samples, we observe that plagioclase grains away from the zone of highly localized strain still preserve their igneous texture (Figures 6b and 7d). Furthermore, pyroxene grains throughout the Ramberg samples show amphibole reaction rims indicating hydration. These microstructural observations, together with results of previous studies on the nucleation of ductile shear zones on brittle precursors (Guermani & Pennacchioni, 1998; Mancktelow & Pennacchioni, 2005; Menegon et al., 2017; Pennacchioni & Mancktelow, 2007; Pittarello et al., 2012; Segall & Simpson, 1986; Tullis et al., 1990), lead to the conclusion that fluids were initially introduced by fracturing causing the formation of amphibole rims around pyroxene and initiating hydrolytic weakening of plagioclase in the vicinity of the fracture (Griggs, 1967; Tullis & Yund, 1980). The observation of hydrolytic weakening of wall-rock plagioclase in the Ramberg samples together with the formation of amphibole-rims around pyroxene documents that deformation took place at amphibolite-facies conditions—conditions at which plagioclase is still stable. It has been recently stated that the thickness of the zone accommodating strain should neither extend nor thicken due to continuous displacement but is predetermined by the compositional and rheological characteristics of the precursory structure (Pennacchioni & Mancktelow, 2018). Because the onset of metamorphic reactions and plastic deformation is mainly controlled by the availability of water together with the observation of a similar thickness of the zones that underwent plastic deformation in RAM-PST and RAM-DSZ of approximately 2 cm (Figures 6 and 7), we assume that the amount of fluid influx was similar in both structures. Chemical analyses of amphibole do not reveal significant variations throughout the thin sections, and we therefore cannot determine whether the fluids were introduced in several episodes or in a single event. In the natural samples, we observe that fluids will trigger reaction and plastic deformation of the reaction products but also cause hydrolytic weakening of plagioclase. Ultimately, a larger rock volume will be affected leading to extensive weakening in the presence of fluids (Ram-PST and RAM-DSZ) relative to situations where free fluids are absent (HAM-PST).

Despite the absence of pseudotachylyte-bearing veins in our experimental samples and the observation of hydrolytic weakening of wall-rock plagioclase at amphibolite-facies conditions in the natural samples, we find some remarkable similarities between the naturally and experimentally produced microstructures. One striking similarity is that the natural and the experimental samples first undergo brittle fracturing (Figures 9a, 9b, 9e, 9f, 11a, 11b, 11e, and 11f). In rather dry environments in nature and in our "as-is" samples, brittle fractures are either preserved, when the rocks did not experience large amounts of shearing (Figures 9a and 9b), or transformed into narrow ductile shear zones due to some reaction when even minor amounts of water are present (Figures 9c–9h). This transformation of brittle fractures into ductile shear zones has been observed and described for different field areas (Guermani & Pennacchioni, 1998; Mancktelow & Pennacchioni, 2005; Menegon et al., 2017; Pennacchioni & Mancktelow, 2007; Pittarello et al., 2012; Segall & Simpson, 1986) and experimentally demonstrated (Tullis et al., 1990; Tullis & Yund, 1985). In our experimental samples deformed with excess water at conditions at which plagioclase is no longer stable, plagioclase transformation spreads along faults and into the adjacent wall rocks, as shown by the low-strain experimental samples. If plagioclase remains a stable phase during deformation conditions, as in the natural Ramberg samples, fluid influx causes hydrolytic weakening of plagioclase and replacement of pyroxene by amphibole (Figures 6 and 7). In the experimental sample as well as in the natural RAM-PST sample, hydration and reaction predominantly occurred on one side of the fault (Figures 6, 9e–9h, and 11a–11f). For the experimental sample, we explain this asymmetry by the exploitation of cleavage planes, mechanical twins, and microcracks as fluid pathways in favorably oriented plagioclase crystals adjacent to the fault (Figure 12). In nature, asymmetric wall-rock damage or wall-rock damage in general is attributed to dynamic shear rupture (Dor et al., 2006; Kim et al., 2004; Mitchell et al., 2011; Rempe et al., 2013; Xu & Ben-Zion, 2017), providing pathways for external fluids to infiltrate the rock triggering retrograde metamorphic reactions at lower crustal depth (Jamtveit et al., 2019; Petley-Ragan et al., 2019). However, given the complex deformation history of the RAM-PST sample, it is also possible that this asymmetry in wall-rock reaction is not caused by preferential reaction in the damage zone associated with the pseudotachylyte vein, but reflects nucleation of a younger pseudotachylyte vein on a preexisting sheared pseudotachylyte or a narrow ductile shear zone (Pittarello et al., 2012).

Our experimental results clearly document that the plastic overprint of brittle fractures is effective in the presence of fluids triggering and sustaining metamorphic reactions causing the accommodation of strain in the reacted rock volumes. In the high-strain sample deformed with water added at 900°C, we observe that the initial brittle structures were completely overprinted by reaction and plastic deformation within only 112 min. Using Li-diffusion chronometry, it has recently been demonstrated that brittle features, for example, pseudotachylytes, in gabbros underwent complete transformation to ductile shear zones during eclogitization in a time span of only a few days to a few months (Smit & Pogge von Strandmann, 2020). Because we imposed temperatures (700°C to 900°C) characteristic for the lower continental crust (650°C to 800°C), we hypothesize that the transition of brittle structures to ductile shear zones may occur within extremely short geological time spans of days to months when hydrous fluids are present in the lower continental crust.

7. Conclusions and Implications

By performing different sets of deformation experiments, in which we independently tested the impact of total strain, water availability, and temperature, we observed the transformation of brittle structures at different stages during deformation. Experimental samples that were deformed with water added reveal a deformation sequence involving initial brittle grain-scale fracturing followed by the influx of hydrous fluids and the subsequent reaction of plagioclase to eclogite-facies minerals. During deformation at 900°C to ~33% axial strain, former brittle structures were completely overprinted by reactions and plastic deformation of the reaction products. Our study highlights the importance of metamorphic reactions for the transformation of brittle structures to ductile shear zones and demonstrates that this transformation is much more efficient in the presence of water triggering and sustaining metamorphic reactions. We also highlight the importance of fluid infiltration into the wall-rock causing reaction and plastic deformation resulting in the widening of the plastically deforming zone. Our experimental microstructures resemble natural microstructures found in compositionally similar rocks that experienced amphibolite to eclogite-facies metamorphism and, therefore, help to understand the sequence of faulting, high-grade metamorphism, and plastic deformation in rocks of the lower continental crust.

Data Availability Statement

The Griggs data and the chemical analyses used for this study can be found in Incel, Sarah; Renner, Jörg; Jamtveit, Bjørn (2020), "Data repository for: Evolution of brittle structures in plagioclase-rich rocks at high-grade metamorphic conditions—Linking laboratory results to field observations", Mendeley Data, v1 (https://doi.org/10.17632/st6m4ccz4m.1).

Acknowledgments
We are very grateful to Neil Mancktelow and an anonymous reviewer for their helpful comments. Special thanks go to Frank Bettenstedt for his help in the lab and to Kristina Dunkel, Arianne Petley-Ragan, François Renard, and Yehuda Ben-Zion for discussions before and during the fieldwork. S. I. received funding from the Alexander von Humboldt Foundation (Feodor Lynen-fellowship).

References

Austrheim, H. (1986). Eclogitization of lower crustal granulites by fluid migration through shear zones. *Earth and Planetary Science Letters*, *81*, 221–232.

Austrheim, H., Dunkel, K. G., Plümper, O., Ildefonse, B., Liu, Y., & Jamtveit, B. (2017). Fragmentation of wall rock garnets during deep crustal earthquakes. *Science Advances*, *3*(2), 1–7. https://doi.org/10.1126/sciadv.1602067

Austrheim, H., & Griffin, W. L. (1985). Shear deformation and eclogite formation within granulite-facies anorthosites of the Bergen Arcs, western Norway. *Chemical Geology*, *50*(1-3), 267–281. https://doi.org/10.1016/0009-2541(85)90124-X

Bhowany, K., Hand, M., Clark, C., Kelsey, D. E., Reddy, S. M., Pearce, M. A., et al. (2017). Phase equilibria modelling constraints on P-T conditions during fluid catalysed conversion of granulite to eclogite in the Bergen Arcs, Norway. *Journal of Metamorphic Geology*, *36*(3), 315–342. https://doi.org/10.1111/jmg.12294

Brace, W. F. (1961). Dependence of fracture strength of rocks on grain size. In The 4th U.S (Ed.), *Symposium on Rock Mechanics (USRMS), 30 March-1 April* (pp. 99–103). Pennsylvania. American Rock Mechanics Association: University Park.

Burnley, P. C., Green, H. W., & Prior, D. J. (1991). Faulting associated with the olivine to spinel transformation in Mg_2GeO_4 and its implications for deep-focus earthquakes. *Journal of Geophysical Research*, *96*(B1), 425–443. https://doi.org/10.1029/90JB01937

Campbell, L. R., & Menegon, L. (2019). Transient high strain rate during localized viscous creep in the dry lower continental crust (Lofoten, Norway). *Journal of Geophysical Research: Solid Earth*, *124*, 10,240–10,260. https://doi.org/10.1029/2019JB018052

Connolly, J. A. D. (1990). Multivariable phase diagrams: An algorithm based on generalized thermodynamics. *American Journal of Science*, *290*(6), 666–718. https://doi.org/10.2475/ajs.290.6.666

Dor, O., Ben-Zion, Y., Rockwell, T. K., & Brune, J. (2006). Pulverized rocks in the Mojave section of the San Andreas Fault Zone. *Earth and Planetary Science Letters*, *245*(3-4), 642–654. https://doi.org/10.1016/j.epsl.2006.03.034

Fredrich, J. T., Evans, B., & Wong, T.-F. (1990). Effect of grain size on brittle and semibrittle strength: Implications for micromechanical modelling of failure in compression. *Journal of Geophysical Research*, *95*(B7), 10,907. https://doi.org/10.1029/jb095ib07p10907

Goldsmith, J. R. (1980). Melting and breakdown reactions of anorthite at high pressures and temperatures. *American Mineralogist*, *65*, 272–284.

Goldsmith, J. R. (1981). The join $CaAl_2Si_2O$-H_2O (anorthite-water) at elevated pressures and temperatures. *American Mineralogist*, *66*, 1183–1188.

Griffin, W. L., Taylor, P. N., Hakkinen, J. W., Heier, K. S., Iden, I. K., Krogh, E. J., et al. (1978). Archaean and Proterozoic crustal evolution in Lofoten-Versterålen, N Norway. *Journal of the Geological Society of London*, *135*(6), 629–647. https://doi.org/10.1144/gsjgs.135.6.0629

Griggs, D. (1967). Hydrolytic weakening of quartz and other silicates. *Geophysical Journal of the Royal Astronomical Society*, *14*(1-4), 19–31. https://doi.org/10.1111/j.1365-246X.1967.tb06218.x

Guermani, A., & Pennacchioni, G. (1998). Brittle precursors of plastic deformation in a granite: An example from the Mont Blanc massif (Helvetic, western Alps). *Journal of Structural Geology*, *20*(2-3), 135–148. https://doi.org/10.1016/S0191-8141(97)00080-1

Hawemann, F., Mancktelow, N., Wex, S., Pennacchioni, G., & Camacho, A. (2019). Fracturing and crystal plastic behaviour of garnet under seismic stress in the dry lower continental crust (Musgrace Ranges, Central Australia). *Solid Earth*, *10*(5), 1635–1649. https://doi.org/10.3929/ethz-a-010782581

Hawemann, F., Mancktelow, N. S., Pennacchioni, G., Wex, S., & Camacho, A. (2019). Weak and slow, strong and fast: How shear zones evolve in a dry continental crust (Musgrave Ranges, Central Australia). *Journal of Geophysical Research: Solid Earth*, *124*, 219–240. https://doi.org/10.1029/2018JB016559

Hawemann, F., Mancktelow, N. S., Wex, S., Camacho, A., & Pennaccioni, G. (2018). Pseudotachylyte as field evidence for lower crustal earthquakes during the intracontinental Petermann Orogeny. *Solid Earth Discussions*, *9*(3), 629–648. https://doi.org/10.5194/se-2017-123

Incel, S., Labrousse, L., Hilairet, N., John, T., Gasc, J., Shi, F., et al. (2019). Reaction-induced embrittlement of the lower continental crust. *Geology*, *47*(3), 235–238. https://doi.org/10.1130/G45527.1

Jamtveit, B., Bucher-Nurminen, K., & Austrheim, H. (1990). Fluid controlled eclogitization of granulites in deep crustal shear zones, Bergen arcs, Western Norway. *Contributions to Mineralogy and Petrology*, *104*(2), 184–193. https://doi.org/10.1007/BF00306442

Jamtveit, B., Petley-Ragan, A., Incel, S., Dunkel, K. G., Aupart, C., Austrheim, H., et al. (2019). The effects of earthquakes and fluids on the metamorphism of the lower continental crust. *Journal of Geophysical Research: Solid Earth*, *124*, 7725–7755. https://doi.org/10.1029/2018JB016461

Jin, Z. M., Zhang, J., Green, I. W., & Jin, S. (2002). Eclogite rheology: Implication for subducted lithosphere. *Geology*, *29*, 667–670. https://doi.org/10.1130/0091-7613(2001)029<0667:ERIFSL>2.0.CO

John, T., Medvedev, S., Rüpke, L. H., Andersen, T. B., Podladchikov, Y. Y., & Austrheim, H. (2009). Generation of intermediate-depth earthquakes by self-localizing thermal runaway. *Nature Geoscience*, *2*(2), 137–140. https://doi.org/10.1038/ngeo419

Jolivet, L., Raimbourg, H., Labrousse, L., Avigad, D., Leroy, Y., Austrheim, H., & Andersen, T. B. (2005). Softening trigerred by eclogitization, the first step toward exhumation during continental subduction. *Earth and Planetary Science Letters*, *237*(3-4), 532–547. https://doi.org/10.1016/j.epsl.2005.06.047

Kim, D., Katayama, I., Michibayashi, K., & Tsujimori, T. (2013). Deformation fabrics of natural blueschists and implications for seismic anisotropy in subducting oceanic crust. *Physics of the Earth and Planetary Interiors*, *222*, 8–21. https://doi.org/10.1016/j.pepi.2013.06.011

Kim, Y. S., Peacock, D. C. P., & Sanderson, D. J. (2004). Fault damage zones. *Journal of Structural Geology*, *26*(3), 503–517. https://doi.org/10.1016/j.jsg.2003.08.002

Kirkpatrick, J. D., & Rowe, C. D. (2013). Disappearing ink: How pseudotachylytes are lost from the rock record. *Journal of Structural Geology*, *52*, 183–198. https://doi.org/10.1016/j.jsg.2013.03.003

Lund, M. G., & Austrheim, H. (2003). High-pressure metamorphism and deep-crustal seismicity: Evidence from contemporaneous formation of pseudotachylytes and eclogite facies coronas. *Tectonophysics*, *372*(1-2), 59–83. https://doi.org/10.1016/S0040-1951(03)00232-4

Lund, M. G., Austrheim, H., & Erambert, M. (2004). Earthquakes in the deep continental crust—Insights from studies on exhumed high-pressure rocks. *Geophysical Journal International*, *158*(2), 569–576. https://doi.org/10.1111/j.1365-246X.2004.02368.x

Mancktelow, N. S., & Pennacchioni, G. (2005). The control of precursor brittle fracture and fluid-rock interaction on the development of single and paired ductile shear zones. *Journal of Structural Geology*, *27*(4), 645–661. https://doi.org/10.1016/j.jsg.2004.12.001

Mansard, N., Stünitz, H., Raimbourg, H., & Précigout, J. (2020). The role of deformation-reaction interactions to localize strain in polymineralic rocks: Insights from experimentally deformed plagioclase-pyroxene assemblages. *Journal of Structural Geology*, *134*, 104008. https://doi.org/10.1016/j.jsg.2020.104008

Marshall, D., & McLaren, A. (1977). Deformation mechanisms in experimentally deformed plagioclase feldspars. *Physics and Chemistry of Minerals*, *1*(4), 351–370. https://doi.org/10.1007/BF00308845

McLaren, A. C., & Pryer, L. L. (2001). Microstructural investigation of the interaction and interdependence of cataclastic and plastic mechanisms in feldspar crystals deformed in the semi-brittle field. *Tectonophysics*, *335*(1-2), 1–15. https://doi.org/10.1016/S0040-1951(01)00042-7

Menegon, L., Pennacchioni, G., Malaspina, N., Harris, K., & Wood, E. (2017). Earthquakes as precursors of ductile shear zones in the dry and strong lower crust. *Geochemistry, Geophysics, Geosystems*, *18*, 4356–4374. https://doi.org/10.1002/2017GC007189

Menegon, L., Stünitz, H., Nasipuri, P., Heilbronner, R., & Svahnberg, H. (2013). Transition from fracturing to viscous flow in granulite facies perthitic feldspar (Lofoten, Norway). *Journal of Structural Geology*, *48*, 95–112. https://doi.org/10.1016/j.jsg.2012.12.004

Milsch, H. H., & Scholz, C. H. (2005). Dehydration-induced weakening and fault slip in gypsum: Implications for the faulting process at intermediate depth in subduction zones. *Journal of Geophysical Research*, *110*, B04202. https://doi.org/10.1029/2004JB003324

Mitchell, T. M., Ben-Zion, Y., & Shimamoto, T. (2011). Pulverized fault rocks and damage asymmetry along the Arima-Takatsuki Tectonic Line, Japan. *Earth and Planetary Science Letters*, *308*(3-4), 284–297. https://doi.org/10.1016/j.epsl.2011.04.023

Moghadam, R. H., Trepmann, C. A., Stöckhert, B., & Renner, J. (2010). Rheology of synthetic omphacite aggregates at high pressure and high temperature. *Journal of Petroleum*, *51*(4), 921–945. https://doi.org/10.1093/petrology/egq006

Okudaira, T., Jerabek, P., Stünitz, H., & Fusseis, F. (2015). High-temperature fracturing and subsequent grain-size-sensitive creep in lower crustal gabbros: Evidence for coseismic loading followed by creep during decaying stress in the lower crust? *Journal of Geophysical Research: Solid Earth*, *120*, 3119–3141. https://doi.org/10.1002/2014JB011708

Pennacchioni, G., & Mancktelow, N. S. (2007). Nucleation and initial growth of a shear zone network within compositionally and structurally heterogeneous granitoids under amphibolite facies conditions. *Journal of Structural Geology*, *29*(11), 1757–1780. https://doi.org/10.1016/j.jsg.2007.06.002

Pennacchioni, G., & Mancktelow, N. S. (2018). Small-scale ductile shear zones: Neither extending, nor thickening, nor narrowing. *Earth-S*, *184*, 1–12. https://doi.org/10.1016/j.earscirev.2018.06.004

Petley-Ragan, A., Ben-Zion, Y., Austrheim, H., Ildefonse, B., Renard, F., & Jamtveit, B. (2019). Dynamic earthquake rupture in the lower crust. *Science Advances*, *5*, eaaw0913. https://doi.org/10.1126/sciadv.aaw0913

Petley-Ragan, A., Dunkel, K. G., Austrheim, H., Ildefonse, B., & Jamtveit, B. (2018). Microstructural records of earthquakes in the lower crust and associated fluid-driven metamorphism in plagioclase-rich granulites. *Journal of Geophysical Research: Solid Earth*, *123*, 3729–3746. https://doi.org/10.1029/2017JB015348

Pittarello, L., Pennacchioni, G., & Di, G. (2012). Tectonophysics amphibolite-facies pseudotachylytes in Premosello metagabbro and felsic mylonites (Ivrea Zone, Italy). *Tectonophysics*, *580*, 43–57. https://doi.org/10.1016/j.tecto.2012.08.001

Poirier, J. P. (1982). On transformation plasticity. *Journal of Geophysical Research*, *87*(B8), 6791–6797. https://doi.org/10.1029/JB087iB08p06791

Price, N. A., Johnson, S. E., Gerbi, C. C., & West, D. P. (2012). Identifying deformed pseudotachylyte and its influence on the strength and evolution of a crustal shear zone at the base of the seismogenic zone. *Tectonophysics*, *518-521*, 63–83. https://doi.org/10.1016/j.tecto.2011.11.011

Raimbourg, H., Jolivet, L., Labrousse, L., Leroy, Y., & Avigad, D. (2005). Kinematics of syneclogite deformation in the Bergen Arcs, Norway: Implications for exhumation mechanisms. *Geological Society of London, Special Publication*, *243*(1), 175–192. https://doi.org/10.1144/GSL.SP.2005.243.01.13

Rempe, M., Mitchell, T., Renner, J., Nippress, S., Ben-Zion, Y., & Rockwell, T. (2013). Damage and seismic velocity structure of pulverized rocks near the San Andreas Fault. *Journal of Geophysical Research: Solid Earth*, *118*, 2813–2831. https://doi.org/10.1002/jgrb.50184

Rybacki, E., & Dresen, G. (2000). Dislocation and diffusion creep of synthetic anorthite aggregates. *Journal of Geophysical Research*, *105*, 17–26.

Rybacki, E., & Dresen, G. (2004). Deformation mechanism maps for feldspar rocks. *Tectonophysics*, *382*, 173–187. https://doi.org/10.1016/j.tecto.2004.01.006

Rybacki, E., Gottschalk, M., Wirth, R., & Dresen, G. (2006). Influence of water fugacity and activation volume on the flow properties of fine-grained anorthite aggregates. *Journal of Geophysical Research*, *111*, B03203. https://doi.org/10.1029/2005JB003663

Rybacki, E., Renner, J., Konrad, K., Herbott, W., Rummel, F., & Stöckhert, B. (1998). A servohydraulically controlled deformation apparatus for rock deformation under conditions of ultra high pressure metamorphism. *Pure and Applied Geophysics*, *152*(3), 579–606. https://doi.org/10.1007/s000240050168

Segall, P., & Simpson, C. (1986). Nucleation of ductile shear zones on dilatant fractures. *Geology*, *14*(1), 56. https://doi.org/10.1130/0091-7613(1986)14<56

Sibson, R. H., & Toy, V. G. (2006). The habitat of fault-generated pseudotachylyte: Presence vs. absence of friction-melt. In R. Abercrombie, et al. (Eds.), *Earthquakes: Radiated energy and the physics of faulting*, *Geophysical Monograph Series* (Vol. 170, pp. 153–166). Washington, DC: American Geophysical Union. https://doi.org/10.1029/170GM16

Smit, M. A., & Pogge von Strandmann, P. A. E. (2020). Deep fluid release in warm subduction zones from a breached slab seal. *Earth and Planetary Science Letters*, *534*, 116046. https://doi.org/10.1016/j.epsl.2019.116046

Steltenpohl, M. G., Kassos, G., & Andresen, A. (2006). Retrograded eclogite-facies pseudotachylytes as deep-crustal paleoseismic faults within continental basement of Lofoten, north Norway. *Geosphere*, *2*(1), 61–72. https://doi.org/10.1130/GES00035.1

Stünitz, H., Fitz Gerald, J. D., & Tullis, J. (2003). Dislocation generation, slip systems, and dynamic recrystallization in experimentally deformed plagioclase single crystals. *Tectonophysics*, *372*(3-4), 215–233. https://doi.org/10.1016/S0040-1951(03)00241-5

Stünitz, H., & Tullis, J. (2001). Weakening and strain localization produced by syn-deformational reaction of plagioclase. *International Journal of Earth Sciences*, *90*(1), 136–148. https://doi.org/10.1007/s005310000148

Trepmann, C. A., & Stöckhert, B. (2002). Cataclastic deformation of garnet: A record of synseismic loading and postseismic creep. *Journal of Structural Geology*, *24*(11), 1845–1856. https://doi.org/10.1016/S0191-8141(02)00004-4

Tribaudino, M., Angel, R. J., Cámara, F., Nestola, F., Pasqual, D., & Margiolaki, I. (2010). Thermal expansion of plagioclase feldspars. *Contributions to Mineralogy and Petrology*, *160*(6), 899–908. https://doi.org/10.1007/s00410-010-0513-3

Tullis, J., Dell'Angelo, L., & Yund, R. (1990). Ductile shear zones from brittle precursors in feldspathic rocks: The role of dynamic recrystallization. *Geophysical Monograph Series*, *56*, 67–81. https://doi.org/10.1029/GM056p0067

Tullis, J., & Yund, R. (1992). The brittle-ductile transition in feldspar aggregates: An experimental study. *International Journal of Geophysics*, *51*, 89–117. https://doi.org/10.1016/S0074-6142(08)62816-8

Tullis, J., & Yund, R. A. (1980). Hydrolytic weakening of experimentally deformed Westerly granite and Hale albite rock. *Journal of Structural Geology*, *2*(4), 439–451. https://doi.org/10.1016/0191-8141(80)90005-X

Tullis, J., & Yund, R. A. (1985). Dynamic recrystallization of feldspar: A mechanism for ductile shear zone formation. *Geology*, *13*(4), 238. https://doi.org/10.1130/0091-7613(1985)13<238:DROFAM>2.0.CO;2

Tullis, J., & Yund, R. A. (1987). Transition from cataclastic flow to dislocation creep of feldspar: Mechanisms and microstructures. *Geology*, *15*(7), 606–609. https://doi.org/10.1130/0091-7613(1987)15<606:TFCFTD>2.0.CO

Wayte, G. J., Worden, R. H., Rubie, D. C., & Droop, G. T. R. (1989). A TEM study of disequilibrium plagioclase breakdown at high pressure: The role of infiltrating fluid. *Contributions to Mineralogy and Petrology*, *101*(4), 426–437. https://doi.org/10.1007/BF00372216

Xu, S., & Ben-Zion, Y. (2017). Theoretical constraints on dynamic pulverization of fault zone rocks. *Geophysical Journal International*, *209*, 282–296. https://doi.org/10.1093/gji/ggx033